Available online at www.sciencedirect.com

SciVerse ScienceDirect

Ceramics International 39 (2013) 8421–8427

CERAMICS INTERNATIONAL

www.elsevier.com/locate/ceramint

Thermal expansion behaviors of yttrium tungstates in the WO_3–Y_2O_3 system

Joon-Ho Koh[a,*], Erinn Sorge[a], Tzu-Chien Wen[b], Dinesh K. Shetty[b]

[a]*Materials and Systems Research, Inc., 5395 W, 700 S, Salt Lake City, UT 84104, USA*

[b]*Department of Materials Science and Engineering, University of Utah, 122 S Central Campus Drive, Salt Lake City, UT 84112, USA*

Received 1 April 2013; received in revised form 2 April 2013; accepted 8 April 2013

Available online 15 April 2013

Abstract

Fully-dense, polycrystalline yttria (Y_2O_3) exhibits high infrared (IR) transmittance in the full mid range (3–5 μm) with low emittance, but lacks thermal-shock resistance for high-performance aerospace applications due to its low strength and high coefficient of thermal expansion (CTE). An attempt was made to develop a low CTE and high strength composite of Y_2O_3 by dispersing the phase, $Y_2W_3O_{12}$, known to exhibit a high negative CTE. The sintered mixture of Y_2O_3 and $Y_2W_3O_{12}$, however, does not form a stable, two-phase composite. The sintered mixture forms new Y_2O_3-rich phases, such as Y_2WO_6 and Y_6WO_{12}, depending on the relative amounts of Y_2O_3 and WO_3. Investigation of the thermal-expansion behaviors of these yttrium tungstates revealed that they have high CTEs comparable to pure Y_2O_3. The goal of obtaining a near-zero CTE composite with Y_2O_3 as the matrix and a yttrium tungstate with a negative CTE as the dispersed phase cannot be realized in this system.

Keywords: Infra-red transparency; Thermal-shock resistance; Low coefficient of thermal expansion; Yttria; Yttrium tungstate

1. Introduction

Polycrystalline Y_2O_3, processed to high density, has attractive optical properties, such as high IR transmittance over the full mid-wavelength range, 3–5 μm, and low emittance at high temperatures [1,2]. However, Y_2O_3 is not as durable in applications involving high temperatures and rapid heating rates as the current material of choice, sapphire [3]. The low durability of Y_2O_3 is due to its low strength and high thermal expansion resulting in low thermal-shock resistance. The average room temperature strength of polycrystalline Y_2O_3 is about 160 MPa, while its average CTE is about 7.5 ppm/°C in the temperature range, 27–727 °C. To increase thermal-shock resistance, strength must be increased and the CTE must be lowered. A modest increase in strength has been achieved recently in Y_2O_3–MgO nanocomposites by sintering nanosized powders at low temperatures and suppressing microstructure coarsening using the dispersed MgO phase, but the CTE of these composites was still too high [4,5]. One approach to achieve both of these goals is to disperse a phase with negative CTE in a Y_2O_3 matrix to achieve a near-zero CTE composite, while the dispersed phase inhibits grain growth and enhances sintering and strength. This approach has been implemented with some success with the negative CTE phase, ZrW_2O_8 [6], dispersed in such matrices as ZrO_2 [7,8] and Al_2O_3 [9]. If a Y_2O_3-rich composite with a dispersed phase with negative CTE can be made to yield a low composite CTE and stable microstructure, it has potential for application in high-speed IR sensor domes and windows.

$Y_2W_3O_{12}$, an orthorhombic phase, is known to exhibit negative CTE with an average linear value of −7.0 ppm/°C in the temperature range, 20–800 °C [10–12]. Yanase et al. [13] fabricated two-phase composites of $Y_2W_3O_{12}$ and $ZrSiO_4$ and obtained a material with an average CTE of −0.08 ppm/°C in the temperature range 25–1000 °C. The two phases were chemically compatible and stable in this temperature range. However, the sintered composite reached a relative density of only 92% of theoretical. Therefore, it is not expected to be IR-transparent in the 3–5 μm range.

Borchardt [14] has reported the existence of five mixed-oxide compounds in the binary system WO_3–Y_2O_3 with the general chemical formula, $WO_3.x(YO_{1.5})$. These five compounds, corresponding to $x=2/3$, 2, 15/4, 9/2 and 6, were

*Corresponding author. Tel.: +1 801 530 4987x18; fax: +1 801 530 4820.
E-mail address: jkoh@msrihome.com (J.-H. Koh).

0272-8842/$ - see front matter © 2013 Elsevier Ltd and Techna Group S.r.l. All rights reserved.
http://dx.doi.org/10.1016/j.ceramint.2013.04.024

Table 1
Various phases from the phase diagram of the WO_3–Y_2O_3 system.

Phase	Stoichiometric formula	Crystal structures and lattice parameters	Melting point	Density (g/cm^3)	CTE (ppm/K, linear avg.)	Reference
Tungsten oxide	WO_3	Monoclinic (a=7.297 Å, b=7.539 Å, c=7.688 Å, β=90.91°)	1473 °C	7.16	10	JCPDS ref. code 01-171-2141
Phase I	$3WO_3 \cdot Y_2O_3$ ($Y_2W_3O_{12}$)	Orthorhombic (a=10.084 Å, b=13.959 Å, c=9.994 Å) Monoclinic (trihydrate, a=14.308 Å, b=4.354 Å, c=12.430 Å, β=119.78°)	1495 °C	4.37–4.97	–7	[10,11,15]
Phase II	$WO_3 \cdot Y_2O_3$ (Y_2WO_6)	Monoclinic (a=7.589 Å, b=5.334 Å, c=11.354 Å, β=104.41°) Orthorhombic (a=8.591 Å, b=20.840 Å, c=5.233 Å)	1700 °C	6.38–6.83	Unknown	[20,22]
Phase III	$8WO_3 \cdot 15Y_2O_3$	N/A	> 2200 °C	6.08		[14]
Phase IV	$4WO_3 \cdot 9Y_2O_3$	N/A	> 2200 °C	5.95		[14]
Phase V	$WO_3 \cdot 3Y_2O_3$ (Y_6WO_{12})	Hexagonal (a=b=9.7505 Å, c=9.3094 Å)	> 2200 °C	5.9–6.0		[14,24]
Yttria	Y_2O_3	Cubic (a=b=c=10.597 Å)	2425 °C	5.01	7	JCPDS ref. code 01-071-5970

designated Phase I, II, III, IV and V, respectively. Table 1 lists these phases and the end components, WO_3 and Y_2O_3, their stoichiometric formulae, crystal structures and lattice parameters, melting temperatures, densities and CTEs where they are known. The end components, WO_3 and Y_2O_3, both have positive CTEs. As noted above, Phase I exhibits a negative CTE. There are no data in the literature on the thermal-expansion behaviors of Phases II, III, IV and V. The phase diagram reported by Borchardt [14] also indicates that Phases II, III, IV and V are not stable below about 1050 °C, thus raising the possibility of $Y_2W_3O_{12}$ (Phase I) and Y_2O_3 existing as two-phase mixtures in a composite.

The present study was undertaken with two motivations. First, it was intended to see if $Y_2W_3O_{12}$ and Y_2O_3 can co-exist as two phases in a composite. If they can co-exist, it opens up an avenue to design and fabricate composites with low CTE. The second motivation was to see if Phases II, III, IV or V can be retained at low temperatures and characterize their CTEs. If one or more of these phases exhibit a negative CTE behavior, they can potentially serve as a negative CTE constituent in a Y_2O_3 matrix to produce a low CTE composite.

2. Experimental

2.1. Powder synthesis and characterization

Powder samples were synthesized by the solid-state reaction route. The starting materials were powders of Y_2O_3 (Alfa Aesar #11181, 99.99%, < 10 μm) and WO_3 (Alfa Aesar #11828, 99.8%, 10–20 μm). The two powders were mixed in the desired molar ratios and milled in a planetary mill (model: PM 400, Retsch Gmbh, Germany) at 400 RPM in butanol for 3 h with spherical zirconia grinding media (1 and 5 mm diameters mixed at 50:50 weight ratio). The media were separated and rinsed after the milling and the butanol was evaporated from the suspension. Compacts of the mixed powders were made using a die press and the powder compacts were calcined in an alumina crucible in air on a powder bed for 2 to 24 h at 1000 or 1100 °C and followed by planetary milling. After the first calcination and milling, the process was repeated.

The resulting powders were analyzed for crystal structure by X-ray diffraction (XRD). Lattice parameters were calculated from the powder XRD data using the software installed in the XRD equipment (X'Pert PW 3040, Phillips). The peaks of the $Y_2W_3O_{12}$ powder samples were compared to those of the orthorhombic phase (JCPDS reference code 01-070-4480) and of the monoclinic form of hydrated $Y_2W_3O_{12} \cdot 3H_2O$ [15]. The XRD peaks of Y_2WO_6 and Y_6WO_{12} powder samples were compared to the peaks reported by Borchardt [14]. The peaks of Y_2O_3 were compared to those of the cubic phase (JCPDS reference code 01-071-5970).

2.2. Fabrication of bars and disks by sintering

The synthesized powders were die-pressed to form bars and disks. The consolidated bars and disks were iso-pressed and sintered in air at temperatures ranging from 1000 to 1650 °C for 2 to 24 h.

Composite samples of Y_2O_3 and $Y_2W_3O_{12}$ were prepared by mixing the two powders at different weight ratios (1:1, 3:1 and 6:1), forming bar specimens, and sintering at different temperatures. These weight ratios correspond to the nominal chemical formula: $WO_3.x(YO_{1.5})$ with x=3.39, 8.83, and 16.99, respectively. If Phases II, III, IV and V are stable only above 1050 °C, then, the three compositions should yield the same weight fractions of Y_2O_3 and $Y_2W_3O_{12}$ in the sintered composite as in the starting powders. If, however, Phases II, III, IV and V are stable down to room temperature, the 1:1 mixture should yield a mixture of Phase II ($WO_3.2YO_{1.5}$) and Phase III ($WO_3.1.875YO_{1.5}$) while the 3:1 and 6:1 mixtures should yield mixtures of Phase V ($WO_3.6YO_{1.5}$) and Y_2O_3. The mixed powders were planetary-milled in butanol at 400 RPM. The dried powders were die-pressed to form bars and cold-isostatic pressed at 245 MPa. The pressed bars were sintered at three different temperatures, 1100 °C (for 20 h),

1500 °C (for 2 h) and 1620 °C (for 2 h) in air. Densities of the sintered bars were measured by the water-immersion method.

Thermal expansion was measured on bar specimens using a dilatometer (WorkHorse™, Anter Corp., Pittsburgh, PA). The data were processed to obtain plots of percent expansion ($100(L-L_0)/L_0$) versus temperature from room temperature (~25 °C) to 800 °C. An average coefficient of thermal expansion (ppm/°C) was calculated from the slope of the thermal-expansion plots.

Pure Y_2O_3 specimens were also prepared as a reference. Fine particles were separated from the as-received yttria powder by a sedimentation process and formed into bars. The bars were sintered at 1650 °C for 2 h in air.

3. Results and discussion

3.1. Structure of $Y_2W_3O_{12}$ and the effect of hydration

The crystal structure of $A_2M_3O_{12}$ family of tungstates and molybdates is ideally orthorhombic, but some members of this family exhibit a phase transition from the orthorhombic to a monoclinic structure on cooling [16]. Examples include $In_2W_3O_{12}$ and $ScInW_3O_{12}$. Associated with this phase transition is a change from negative thermal expansion for the orthorhombic phase at high temperatures to a positive thermal expansion for the monoclinic phase at low temperatures. While many of the past studies on $Y_2W_3O_{12}$ generally agree on the orthorhombic structure (space group: *Pnca*), a few studies reported the presence of a monoclinic phase [15,17]. Kol'tsova [15] claimed that yttrium tungstate exists in the form of a tryhydrate, $Y_2W_3O_{12}\cdot 3H_2O$, having a monoclinic structure (*P*2/*m*). Sleight [17] reported that the room-temperature diffraction pattern of the hydrated $Y_2W_3O_{12}$ phase can be indexed with the monoclinic phase, but it can be converted to a pseudo-orthorhombic phase which is comparable to the room-temperature orthorhombic phase of unhydrated $Y_2W_3O_{12}$. These past studies indicate that $Y_2W_3O_{12}$ may exist in either the orthorhombic (unhydrated) or the monoclinic (hydrated) phase or a mixed phase depending on the degree of hydration.

Fig. 1 shows the XRD patterns of the synthesized $Y_2W_3O_{12}$ powders in comparison with the reference peaks of the orthorhombic and the monoclinic phases. In general, the powder XRD patterns do not show exact matches to either the orthorhombic phase or the monoclinic phase. It appears that all the synthesized $Y_2W_3O_{12}$ powders have mixed phases. The hydration of $Y_2W_3O_{12}$ is known to occur quickly, and no special treatment was employed to prevent hydration of these powders.

Rapid hydration of $Y_2W_3O_{12}$ when exposed to air at room temperature was consistently observed in the past studies. Dehydration occurs when it is heated to 100–200 °C. Sumithra and Umarji [18] reported the relationship between hygroscopicity and structure after analyzing hydrated and dehydrated samples. Dehydrated samples were prepared by heating to 150 °C and cooling in vacuum to room temperature. Unit cell parameters obtained from XRD showed the unit cell volume of a trihydrate ($Y_2W_3O_{12}\cdot 3H_2O$) at room temperature to be 1303 Å^3, while that of an unhydrated form was 1404 Å^3.

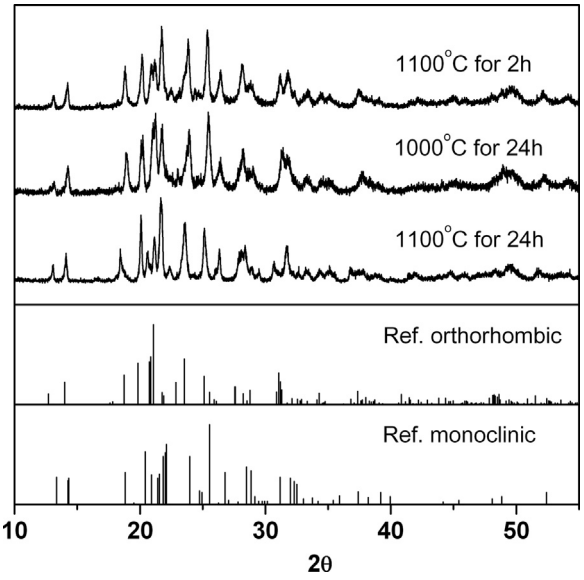

Fig. 1. XRD of $Y_2W_3O_{12}$ powders calcined at different conditions in comparison to the orthorhombic phase reference (JCPDS 01-070-4480) and the monoclinic phase reference ([15]).

The theoretical density of a trihydrate is 4.97 g/cm^3 while that of an unhydrated form is 4.36 g/cm^3. Their thermal-expansion curves showed an initial expansion (up to ~150 °C), apparently due to the removal of water molecules, followed by contraction upon further heating above ~150 °C. The negative thermal expansion behavior of $Y_2W_3O_{12}$ is known to be caused by the transverse thermal vibration, which reduces the apparent metal-oxygen distance (not the true distance), and the presence of water molecules appears to hinder this motion preventing negative thermal expansion. According to their thermo-gravimetric analysis (TGA) studies, the stable hydration number (x) for $Y_2W_3O_{12}\cdot xH_2O$ is approximately 3, but it can be lower depending on storage conditions which alter the degree of hydration.

3.2. Sintering and thermal expansion of $Y_2W_3O_{12}$

The sintered $Y_2W_3O_{12}$ specimens are expected to have the orthorhombic structure as dehydration should occur during the heating. However, the sintered specimens may transform to the monoclinic phase or mixed phases when cooled to room temperature in air.

Table 2 lists the sintering conditions and the measured densities of sintered $Y_2W_3O_{12}$ specimens. The densities listed in Table 2 are less than the theoretical crystal densities calculated using the formula units per unit cell and the lattice parameters due to residual porosity. It is also possible that some loss of WO_3 occurs during sintering (especially at high temperatures). This can lead to the formation of Y_2O_3-rich phases that generally have higher theoretical densities. Poor sinterability of $Y_2W_3O_{12}$ due to sublimation of WO_3 was addressed by Sumithra and Umarji [19].

Fig. 2 shows the linear thermal expansion of $Y_2W_3O_{12}$ sintered at 1400 °C for 2 h. The expansion curve shows an

initial positive expansion up to ~200 °C followed by a negative expansion from 200 to 800 °C. The average CTE in the negative expansion temperature range, 200–800 °C, was −7.5 ppm/K which is close to the literature values [10–12]. The shift from positive to negative expansion is similar to reports of earlier studies, and it is due to dehydration and the phase transition from monoclinic-to-orthorhombic structure.

3.3. Structure and thermal expansion of sintered Y_2O_3–$Y_2W_3O_{12}$ composites

Table 3 summarizes the measured densities of the Y_2O_3–$Y_2W_3O_{12}$ composite specimens sintered at three different temperatures: 1100, 1500 and 1620 °C. Also listed in the table are the theoretical densities based on the volume fractions and the theoretical densities of the Y_2O_3 (cubic) and the $Y_2W_3O_{12}$ (orthorhombic) phases. The measured densities increased significantly with the sintering temperature for all

Table 2
Sintering conditions and measured densities of the sintered $Y_2W_3O_{12}$ specimens.

Temperature	Hours	Density (g/cm^3)	Open porosity
1000 °C	24	4.047	0.207
1100 °C	24	4.040	0.215
1200 °C	2	4.448	0.295
1300 °C	2	4.588	0.103
1400 °C	2	4.456	0.322
1500 °C	2	4.471	0.279

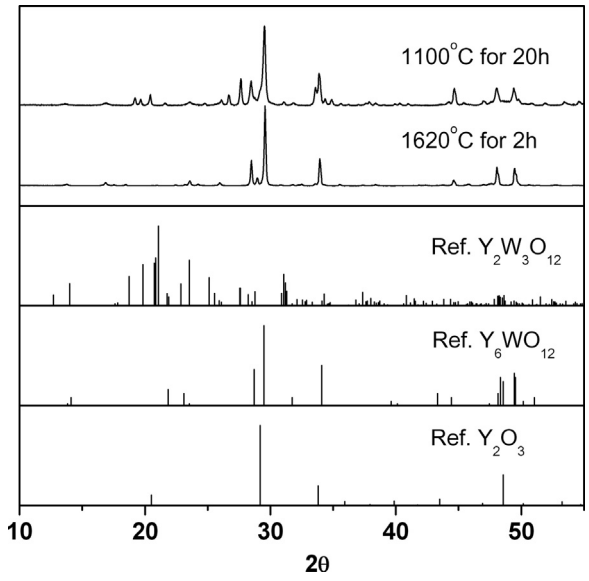

Fig. 3. XRD of the sintered Y_2O_3–$Y_2W_3O_{12}$ composite samples (1:1 by weight) in comparison to the $Y_2W_3O_{12}$ orthorhombic phase reference (JCPDS 01-070-4480), the Y_6WO_{12} phase reference ([14]), and the Y_2O_3 phase reference (JCPDS 01-071-5970).

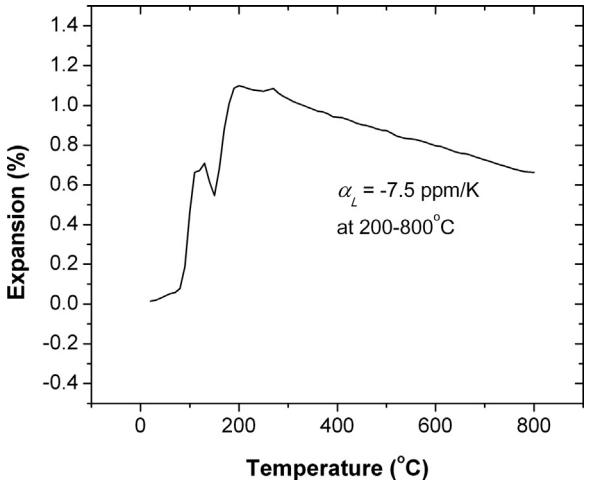

Fig. 2. Thermal expansion curve of the $Y_2W_3O_{12}$ sample sintered at 1400 °C for 2 h.

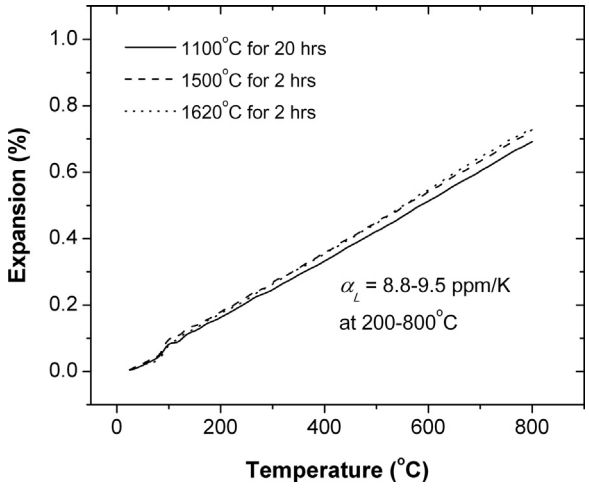

Fig. 4. Thermal expansion curves of Y_2O_3–$Y_2W_3O_{12}$ composite samples (1:1 wt.) sintered at different temperatures.

Table 3
Measured densities (g/cm^3) of Y_2O_3–$Y_2W_3O_{12}$ composite specimens.

Composition (Y_2O_3:$Y_2W_3O_{12}$)	Sintered at 1100 °C for 20 h	Sintered at 1500 °C for 2 h	Sintered at 1620 °C for 2 h
1:1 wt. ratio TD=4.685 g/cm^3	3.394	4.007	5.513
3:1 wt. ratio TD=4.842 g/cm^3	3.188	3.760	4.614
6:1 wt. ratio TD=4.913 g/cm^3	3.076	3.924	4.799

Table 4
Linear CTE of the sintered Y_2O_3–$Y_2W_3O_{12}$ composite specimens.

Composition (Y_2O_3:$Y_2W_3O_{12}$)	Sintered at 1100 °C for 20 h	Sintered at 1500 °C for 2 h	Sintered at 1620 °C for 2 h
1:1 wt. ratio	8.853	9.178	9.467
3:1 wt. ratio	8.542	9.247	9.289
6:1 wt. ratio	8.062	8.679	8.679

three phase mixtures. Generally, the measured densities were lower than the theoretical densities. One exception was the 1:1 (wt.) composite sintered at 1620 °C which showed a much higher measured density (5.5 g/cm^3) than the theoretical (4.7 g/cm^3). Note that the Y_2O_3-rich phases (e.g. Phases II, III, IV, and V in Table 1) have higher densities (5.9–6.6 g/cm^3) than $Y_2W_3O_{12}$ (Phase I). The higher-than-theoretical density may indicate that the composite forms another phase when sintered at high temperatures.

The XRD patterns of the composite samples sintered at 1100 °C and 1620 °C are shown in Fig. 3 in comparison to the reference peaks of $Y_2W_3O_{12}$ (Phase I, orthorhombic), Y_6WO_{12} (Phase V), and Y_2O_3. The XRD pattern of the composite sintered at 1500 °C (not shown in Fig. 3) was the same as that sintered at 1620 °C. The diffraction pattern of the composite sintered 1620 °C indeed matched the peaks of Y_6WO_{12} (Phase V). The $Y_2W_3O_{12}$ phase disappeared almost completely. Even the composite sintered at 1100 °C showed no evidence of the $Y_2W_3O_{12}$ phase. Apparently, the negative-thermal-expansion $Y_2W_3O_{12}$ phase is unstable in the sintered mixture of Y_2O_3–$Y_2W_3O_{12}$. The diffraction pattern of the sintered mixtures resembles that of the Y_2O_3-rich phases. A stable composite consisting of Y_2O_3 (positive CTE) and $Y_2W_3O_{12}$ (negative CTE) does not form. These results also suggest that Y_6WO_{12} can be retained at room temperature after sintering at high temperatures. It is yet to be established, however, if Y_6WO_{12} is stable or metastable at room temperature.

The thermal expansion curves of the sintered Y_2O_3–$Y_2W_3O_{12}$ composites are shown in Fig. 4. The anticipated low thermal expansion behavior was not observed, due to non-existence of the negative-thermal-expansion $Y_2W_3O_{12}$ phase, as confirmed from the XRD results. The thermal expansion results showed that the sintered Y_2O_3–$Y_2W_3O_{12}$ composites exhibit a thermal-expansion behavior close to that of pure yttria. The sintering temperature had no influence on the resulting crystalline phases and the thermal-expansion behavior. The thermal-expansion plots of the specimens with the 3:1 and 6:1 compositions showed behaviors similar to those shown in Fig. 4. The average CTE values of all the samples are listed in Table 4. The average CTE was in the range of 8.0–9.5 ppm/K in the temperature range, 20–800 °C.

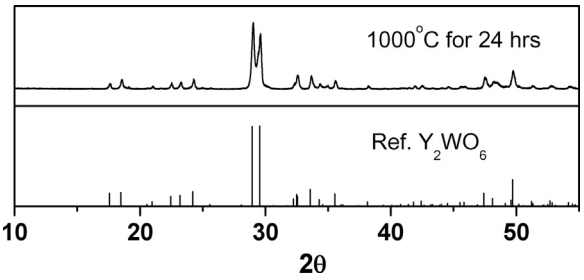

Fig. 5. XRD of Y_2WO_6 powder in comparison to the Y_2WO_6 phase reference (JCPDS 01-073-0118).

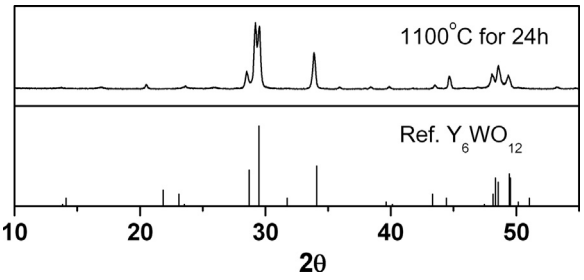

Fig. 6. XRD of Y_6WO_{12} powder in comparison to the Y_6WO_{12} phase reference ([14]).

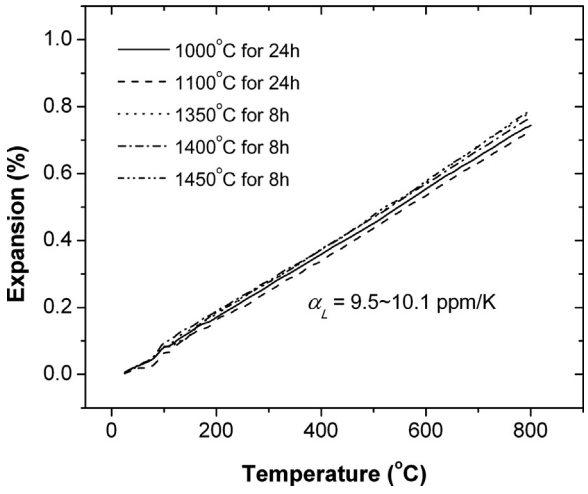

Fig. 7. Thermal expansion curves of Y_2WO_6 samples sintered at different temperatures.

3.4. Structure and thermal expansion of Y_2WO_6 and Y_6WO_{12}

Yttrium oxytungstate, Y_2WO_6 or $Y_2O_3 \cdot WO_3$, referred to as Phase II by Borchardt [14], was prepared by the solid-state reaction method. Y_2WO_6 is known to have a stable monoclinic structure [20,21], but some metastable phases such as the orthorhombic phase were also claimed in the past [22,23].

The synthesized powder was examined using XRD and compared to the monoclinic phase, as shown in Fig. 5.

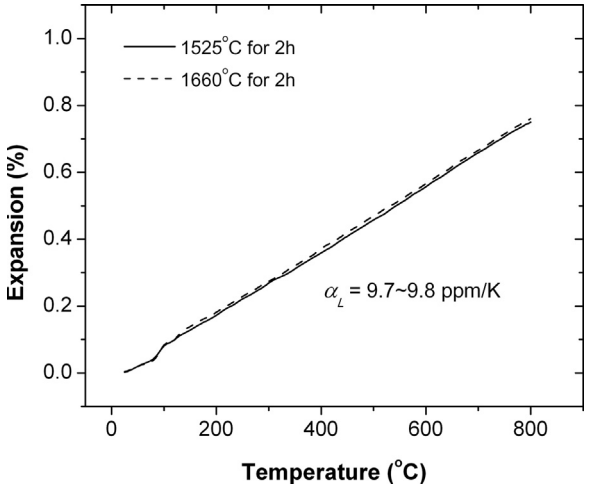

Fig. 8. Thermal expansion curves of Y_6WO_{12} samples sintered at different temperatures.

Table 5
Linear CTE of the sintered Y_2WO_6 and Y_6WO_{12} specimens.

Specimen	Sintering condition	Linear CTE
Y_2WO_6 (Phase II)	1000 °C for 24 h	9.584
	1100 °C for 24 h	9.490
	1350 °C for 8 h	10.019
	1400 °C for 8 h	9.710
	1450 °C for 8 h	10.118
Y_6WO_{12} (Phase V)	1525 °C for 2 h	9.703
	1660 °C for 2 h	9.793

The powder XRD peaks matched those of the reference very closely. The monoclinic phase appears to be stable and easily synthesized.

Y_6WO_{12} (Phase V), was prepared similarly and analyzed for its crystalline structure using XRD. This phase is known to have a high melting temperature (>2200 °C) and exists in the rhombohedral structure at 1700 °C or below. The powder XRD of Y_6WO_{12} matched the reference very closely as shown in Fig. 6.

The thermal expansion curves of Y_2WO_6 and Y_6WO_{12} samples are shown in Figs. 7 and 8, respectively. The average CTE values in the temperature range, 20–800 °C, are listed in Table 5.

The CTEs of both Y_2WO_6 and Y_6WO_{12} are positive and the average CTE values are greater than that of Y_2O_3. These materials are not expected to be useful for a composite with Y_2O_3 to make a low CTE material.

4. Conclusions

Among the known phases in the WO_3–Y_2O_3 system, only $Y_2W_3O_{12}$ ($3WO_3 \cdot Y_2O_3$) exhibits the negative thermal expansion behavior. All other Y_2O_3-rich phases, including Y_2WO_6 and Y_6WO_{12} have high positive coefficients of thermal expansion.

The sintered mixture of Y_2O_3–$Y_2W_3O_{12}$ does not form a stable, low-thermal-expansion composite, despite the large negative CTE of $Y_2W_3O_{12}$. The sintered mixture forms an Y_2O_3-rich phase which has a large positive CTE. A near-zero thermal expansion composite with Y_2O_3 matrix is not obtainable from the WO_3–Y_2O_3 system.

References

[1] D.C. Harris, Materials for Infrared Windows and Domes—Properties and Performance, SPIE Optical Engineering Press, Bellingham, Washington, 1999.
[2] D.C. Harris, Durable 3–5 μm transmitting infrared window materials, Infrared Physics and Technology 39 (1998) 185–201.
[3] P. Hogan, T. Stefanik, C. Willingham, R. Gentilman, Transparent yttria for IR windows and domes—past and present, in: Proceedings of the 10th DoD Electromagnetic Windows Symposium, Norfolk, VA, May 19th 2004.
[4] T. Stefanik, R. Gentilman, P. Hogan, Nanocomposite optical ceramics for infrared windows and domes, Proceedings of SPIE 6545 (2007) 65450A1–65450A5.
[5] J. Wang, D. Chen, E.H. Jordan, M. Gell, Infrared-transparent Y_2O_3–MgO nanocomposites using sol–gel combustion synthesized powder, Journal of the American Ceramic Society 93 (2010) 3535–3538.
[6] T.A. Mary, J.S.O. Evans, T. Vogt, A.W. Sleight, Negative thermal expansion from 0.3 to 1050 K in ZrW_2O_8, Science 272 (1996) 90–92.
[7] P. Lommens, C. De Meyer, E. Bruneel, K. De Buysser, I. van Driessche, S. Hoste, Synthesis and thermal expansion properties of ZrO_2/ZrW_2O_8 composites, Journal of the European Ceramic Society 25 (2005) 3605–3610.
[8] X. Yang, J. Xu, H. Li, X. Cheng, X. Yan, In situ synthesis of ZrO_2/ZrW_2O_8 composites with near-zero thermal expansion, Journal of the American Ceramic Society 90 (2007) 1953–1955.
[9] L. Sun, A. Sneller, P. Kwon, ZrW_2O_8-containing composites with near-zero coefficient of thermal expansion fabricated by various methods: comparison and optimization, Composites Science and Technology 68 (2008) 3425–3430.
[10] P.M. Foster, A.W. Sleight, Negative thermal expansion in $Y_2W_3O_{12}$, International Journal of Inorganic Materials 1 (1999) 123–127.
[11] D.A. Woodcock, P. Lightfoot, C. Ritter, Negative thermal expansion in $Y_2(WO_4)_3$, Journal of Solid State Chemistry 149 (2000) 92–98.
[12] S. Sumithra, A.K. Tyagi, A.M. Umarji, Negative thermal expansion in $Er_2W_3O_{12}$ and $Y_2W_3O_{12}$ by high temperature X-ray diffraction, Materials Science and Engineering: B 116 (2005) 14–18.
[13] I. Yanase, M. Miyagi, H. Kobayashi, Fabrication of zero-thermal-expansion $ZrSiO_4$/$Y_2W_3O_{12}$ sintered body, Journal of the European Ceramic Society 29 (2009) 3129–3134.
[14] H.J. Borchardt, Yttrium-tungsten oxides, Inorganic Chemistry 2 (1963) 170–173.
[15] T.N. Kol′tsova, X-ray diffraction study of $Y_2W_3O_{12} \cdot 3H_2O$, Inorganic Materials 37 (2001) 1175–1177.
[16] T.A. Mary, A.W. Sleight, Bulk thermal expansion for tungstates and molybdates of the type $A_2M_3O_{12}$, Journal of Materials Research 14 (1999) 912–915.
[17] A.W. Sleight, Negative thermal expansion, Materials Research Society Symposium Proceedings, vol. 755 2003, DD10.6.1.
[18] S. Sumithra, A.M. Umarji, Role of crystal structure in the thermal expansion of $Ln_2W_3O_{12}$ (Ln=La, Nd, Dy, Y, Er and Yb), Solid State Sciences 6 (2004) 1313–1319.
[19] S. Sumithra, A.M. Umarji, Hygroscopicity and bulk thermal expansion in $Y_2W_3O_{12}$, Materials Research Bulletin 40 (2005) 167–176.
[20] V.A. Efremov, A.V. Tyulin, V.K. Trunov, O.V. Kudin, V.K. Yanovskii, V.I. Voronkova, Crystal structure of monoclinic Y_2WO_6 and Yb_2WO_6, Soviet Physics Crystallography 29 (1984) 534–537.

[21] J. Wang, Z.-J. Zhang, J.-T. Zhao, H.-H. Chen, X.-X. Yang, Y. Tao, Y. Huang, Luminescent metastable Y_2WO_6:Ln^{3+} (Ln=Eu, Er, Sm, and Dy) microspheres with controllable morphology *via* self-assembly, Journal of Materials Chemistry 20 (2010) 10894–10900.

[22] O. Beaury, M. Faucher, G.T. De Sagey, The structure of yttrium tungstate ε-Y_2WO_6, Acta Crystallographica Section B: Structural Science 37 (1981) 1166–1170.

[23] A.V. Tyulin, V.A. Efremov, V.K. Trunov, Polymorphism of oxytungstates TR_2WO_6. Mechanisms of structural changes in Y_2WO_6, Soviet Physics Crystallography 34 (1989) 531–536.

[24] N. Diot, P. Benard-Rocherulle, R. Marchand, X-ray powder diffraction data and Rietveld refinement for Ln_6WO_{12}(Ln=Y,Ho), Powder Diffraction 15 (2000) 220–226.